Vortex solitons in an off-resonant Raman medium

A. V. Gorbach and D. V. Skryabin
Centre for Photonics and Photonic Materials, Department of Physics, University of Bath, Bath BA2 7AY, United Kingdom

C. N. Harvey
School of Mathematics and Statistics, University of Plymouth, Plymouth PL4 8AA, United Kingdom

(Received 13 March 2008; published 10 June 2008)

We investigate the existence and linear stability of coupled vortex solitons supported by cascaded four-wave mixing in a Raman active medium excited away from the resonance. We present a detailed analysis for the two- and three-component vortex solitons and demonstrate the formation of stable and unstable vortex solitons, and associated spatiotemporal helical beams, under the conditions of the simultaneous frequency and vortex comb generation.

DOI: 10.1103/PhysRevA.77.063810 PACS number(s): 42.65.Tg, 42.50.Gy, 05.45.Yv, 42.65.Ky

I. INTRODUCTION

Optical vortices are point phase singularities of the electromagnetic field, with the beam intensity vanishing at the singularity and the field phase changing by $2\pi l$ along any closed loop around it. $l=0,\pm 1,\pm 2,\ldots$ is known as the orbital angular momentum quantum number or vortex charge. In a nonlinear medium vortices can propagate undistorted due to a balance between diffraction and nonlinearity, and form so-called vortex solitons [1]. Nonlinearity can also trigger frequency conversion accompanied by the conversion of the charge l. In particular, in the second-order harmonic generation process, the fundamental field carrying a vortex with the charge l is converted into the second-order harmonic field with the charge $2l$ [1–6]. Analogous conversion rules have been reported for the degenerate four-wave mixing in Kerr-like materials [7] and for the three-wave Raman resonant process [8]. Multicomponent vortex solitons sustained by the interaction of the beams with different frequencies in both quadratic and cubic materials are also well known, though under the most typical conditions the finite radius vortex solitons break into filaments due to azimuthal instabilities [1,2,4,5].

While the above-mentioned experimental and theoretical research of nonlinear vortex charge conversion has focused on cases involving a small number of frequency components, typically two or three, the efforts directed toward short pulse generation have resulted in the development of techniques leading to the generation of dozens of coherent frequency sidebands, by means of cascaded four-wave mixing in Raman active gases [9,10]. The latter technique does not rely on the waveguide or cavity geometries to boost nonlinear interaction and is therefore suitable for the simultaneous frequency and vortex charge conversion. This idea has been explored by our group and we have recently demonstrated simultaneous generation of frequency and vortex combs [11] in a Raman medium excited off-resonance with the two pump beams, when one of the two carries a unit vortex and the other is vortex free. We have derived the vortex conversion rules and demonstrated that the simultaneous frequency and vortex combs are shaped in the form of the spatiotemporal helical beams [11]. On the focusing side of the Raman resonance, the multicomponent vortex solitons have been found.

The aim of this work is to report regular tracing of the multicomponent vortex solitons in the parameter space and to study their linear stability with respect to perturbations. Our analysis shows that the spectrally symmetric soliton solutions centered around the vortex-free frequency component are typically unstable, although the instability fully develops only after long propagation distances. At the same time, the asymmetric solitons, for example those where all the generated components are the Stokes ones, have a broad stability range. Based on the results of the linear stability analysis for two and three component solitons, we demonstrate the same general tendencies of the soliton dynamics for the case of many coupled sidebands.

II. MODEL

The dimensionless model describing the evolution of the sidebands in an off-resonantly excited Raman medium is [9,11]

$$i\partial_z E_n - \frac{1}{2}\Delta E_n = \beta_n E_n + Q^* E_{n-1} + Q E_{n+1}, \tag{1}$$

where $n=-M+1,\ldots,0,\ldots,N$ $(M,N\geq 0)$, and $\Delta=\partial_x^2+\partial_y^2$. E_n are the dimensionless amplitudes of the sidebands, such that the total field is given by

$$E_{\mathrm{tot}}=\sum_n E_n(x,y,z)e^{i\Omega_n t-iK_n z}, \tag{2}$$

where $\Omega_n=(\omega_0+n\omega_{\mathrm{mod}})/\omega_{\mathrm{mod}}$, $\omega_{\mathrm{mod}}=\omega_1-\omega_0$ is the modulation frequency (i.e., the frequency difference between the two driving fields). N is the number of the anti-Stokes components and $M-1$ is the number of the Stokes components. Taking into account the E_0 field, we have $M+N$ interacting Raman sidebands. The physical frequencies and wave numbers are represented by the lower case letters ω_n and k_n, while their dimensionless counterparts by the upper case: Ω_n and K_n. The dimensionless time t is measured in units of $1/\omega_{\mathrm{mod}}$, the propagation coordinate z is in units of L, and the transverse coordinates (x,y) are in units of $\sqrt{Lc/\omega_0}$. $K_n=(\omega_0+n\omega_{\mathrm{mod}})L/c$ are the scaled free space wave numbers. Here, $L=(\eta\hbar\omega_0\mathcal{N}|b|)^{-1}$ characterizes the coupling length

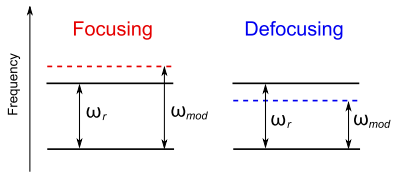

FIG. 1. (Color online) Off-resonant excitations of the Raman transition creating either focusing or defocusing nonlinearities. ω_r is the Raman frequency and $\omega_{\mathrm{mod}}=\omega_1-\omega_0$, where $\omega_1>\omega_0$ are the pump frequencies.

over which power is transferred between neighboring sidebands in the absence of dispersion. $\eta\approx 376$ is the free space impedance, $\mathcal{N}$ is the density of molecules, and b is a coefficient characterizing the material dependent coupling between the sidebands [9]. The weak frequency dependence of b is neglected for simplicity.

L varies from 1 to a few mm for D_2 and H_2 gases [9], so that one unit of x corresponds to a few tens of microns. Q is the Raman coherence responsible for the coupling between the sidebands. Neglecting dissipation due to finite linewidth of atomic transition and finite dephasing time, in the adiabatic approximation [9,11,12]

$$Q(E_n)=\frac{\mathrm{sgn}(\mu)S}{2\sqrt{\mu^2+|S|^2}},\quad S=\sum_n E_n E_{n+1}^*, \tag{3}$$

where $\mu=|\omega_{\mathrm{mod}}-\omega_r|/(|b|I_0)$ is the scaled modulus of the detuning of the modulation frequency from the Raman frequency ω_r. We also note that the above result is obtained under the assumption of equal Stark shifts of molecular levels, which is the case for large detunings [9]. While $|\mu|$ can always be fixed to unity by proper rescaling of the field amplitudes, its sign controls the effective type of nonlinearity in Eqs. (1): positive (negative) μ corresponds to the focusing (defocusing) nonlinearity [11,13], see Fig. 1. In what follows we consider the case of the focusing nonlinearity [13,14], ($\mu=1$), which is known to support bright soliton solutions [15,16].

$|Q|$ varies from 0 to 1/2 for $|S|/\mu$ varying from 0 to ∞. Therefore nonlinear interaction between harmonics is saturated at high powers or, equivalently, at small detunings $|\omega_{\mathrm{mod}}-\omega_r|$. $E_n\sqrt{I_0}$ are the dimensional amplitudes of the harmonics. For D_2 and H_2 gases $\mu=1$ corresponds to $I_0\sim 0.1$ GW/cm^2, provided $|\omega_{\mathrm{mod}}-\omega_r|\sim 1$ GHz. $\beta_n\equiv\beta(\omega_n)$ is the propagation constant of the nth harmonic.

III. SOLITON SOLUTIONS: GENERAL FRAMEWORK

In this and the next chapter we describe the general framework for finding the stationary soliton solutions and studying their linear stability. Application of these techniques to the cases of two and three components are described in detail in Secs. V and VI. The fact that Eqs. (1) and (3) are invariant with respect to $E_n\to E_n\exp(i\phi)$ and $E_n\to E_n\exp(in\psi)$, where ϕ and ψ are arbitrary constants [11,12], implies the conservation of the two integrals $P=\Sigma_n I_n$ and $R=\Sigma_n n I_n$, where $I_n=\iint dxdy|E_n|^2$, and suggests the following ansatz for the soliton solutions:

$$E_n(x,y,z)=f_n(r)\exp[il_n\theta+i(\kappa_1+\kappa_2 n)z]. \tag{4}$$

Here r and θ are the polar radius and angle, $l_n=l_0+n(l_1-l_0)$ is the vortex charge of the nth harmonic, and $\kappa_{1,2}$ are free parameters associated with the above symmetries. The choice of l_0 and l_1 defines the step, $\Delta l=l_1-l_0$, in which the vortex charge is changing between the adjacent sidebands. $f_n(r)$ are real functions obeying

$$-\frac{1}{2}\left[\frac{d^2f_n}{dr^2}+\frac{1}{r}\frac{df}{dr}-\frac{l_n^2}{r^2}f_n\right]=[\kappa_1+\kappa_2 n+\beta_n]f_n+q(f_{n-1}+f_{n+1}), \tag{5}$$

where $q=Q(f_n)$. The boundary conditions are [4]

$$f_n(r)\to c_n^{(0)}r^{|l_n|},\quad r\to 0, \tag{6}$$

$$f_n(r)\to c_n^{(\infty)}\frac{e^{-r\sqrt{-2(\kappa_1+\kappa_2 n+\beta_n)}}}{\sqrt{r}},\quad r\to\infty, \tag{7}$$

where $c_n^{(0,\infty)}$ are real constants. Equation (6) naturally implies that the amplitude of a vortex carrying component $l_n\neq 0$ is zero at the phase singularity and that the vortex free components $l_n=0$ reach some constant value at $r=0$. For the fields to decay to zero at $r\to\infty$, one needs to select $\kappa_{1,2}$ to satisfy

$$\kappa_1+\kappa_2 n+\beta_n<0 \tag{8}$$

simultaneously for all n. Without any loss of generality β_0 can always be set to zero by the rotation of the common phase [11]. Thus, fixing $\beta_0=0$ we find that the above inequality for $n=0$ gives $\kappa_1<0$. At the boundary points of the above conditions f_n tends to zero. Detuning the $\kappa_{1,2}$ values away from these boundaries into the range where I_n is increasing eventually leads to the coherence tending to its maximal value $q=1/2$. Examples of the radial profiles of the vortex solitons are shown in Fig. 2 for the asymmetric configuration with only Stokes components being excited ($N=0$). When the propagation constants β_n are symmetric around the central component: $\beta_n=\beta_{-n}$, Eq. (5) are invariant under the transformation $n\to -n$, $\kappa_2\to-\kappa_2$, $l_n\to -l_n$. In this case solitons in the opposite configuration, with only anti-Stokes components being excited ($M=1$), have exactly the same structure as those shown in Fig. 2.

In the vortex soliton case the $q=1/2$ limit is achieved not only through the growing amplitudes, but also through the expansion of the rings and flattening of their profiles. The soliton existence boundary corresponding to $q=1/2$ can be worked out neglecting the x and y dependence of E_n. Subsequently one can disregard the left-hand sides in Eq. (5), assume $q=1/2$ and work out constraints on the κ_1 and κ_2 values from the solvability conditions of the resulting homogeneous equations $[\kappa_1+\kappa_2 n+\beta_n]f_n+(f_{n-1}+f_{n+1})/2=0$. Examples of the existence domains in the (κ_1,κ_2) plane can be seen in Figs. 3(a) and 7.

IV. LINEAR STABILITY ANALYSIS: GENERAL FRAMEWORK

Stability of the vortex solutions is of course an important problem, since similar solutions in other models are known

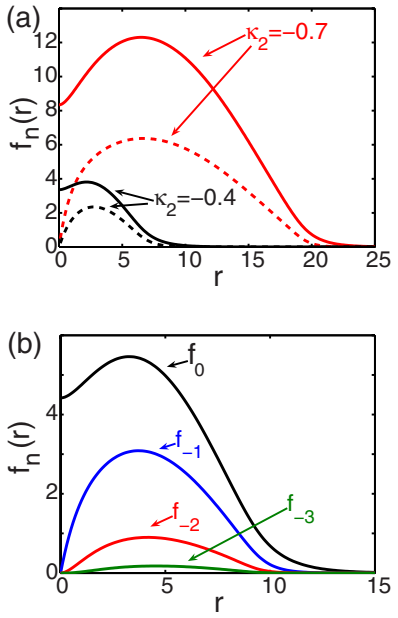

FIG. 2. (Color online) Soliton radial profiles for the configuration with only Stokes components being excited ($N=0$), $\beta_n=0.005n^2$ (which corresponds to normal dispersion), charge conversion step is unity: $l_n=n$. (a) Two coupled fields ($M=2$), $\kappa_1=-0.25$, $\kappa_2=-0.4$ (black curves), $\kappa_2=-0.7$ [red (gray) curves]. Solid (dashed) curves correspond to f_0 (f_{-1}); (b) five coupled fields ($M=5$), $\kappa_1=-0.25$, $\kappa_2=-0.7$.

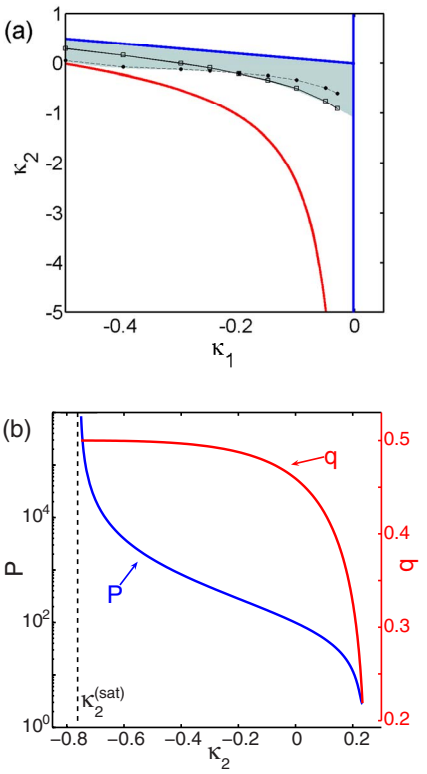

FIG. 3. (Color online) (a) Region of existence of coupled vortex solitons for the case of two fields, $\beta_1=0.005$. Straight blue lines correspond to the boundaries of existence in Eq. (8), red (gray) curve–to the dispersion $\kappa_2^{(\mathrm{sat})}$ of high-intensity constant amplitude waves, Eq. (20). Shaded area indicates region of unstable solutions for the configuration ($l_0=0$, $l_1=1$), open squares and filled circles correspond to numerically found instability thresholds for the $J=1$ and $J=2$ unstable perturbations, respectively (see main body text for details and Figs. 4–6). (b) Soliton power P and maximum value of the coherence q versus κ_2 at fixed value of $\kappa_1=-0.25$. Approaching the boundary $\kappa_2^{(\mathrm{sat})}(\kappa_1)$ q is saturated at its maximum value $|q|=0.5$, while the norm tends to infinity.

to exhibit strong modulational instability along the rings [4,5,17]. This instability can be suppressed by nonlocal nonlinearities [18,19], and in some cases when the higher order nonlinearities (e.g., quintic) are assumed to dominate over the lower order ones (e.g., cubic), see, e.g., Refs. [7,20]. Our model is particularly interesting because, as we will demonstrate below, it allows the existence of a sufficiently broad parameter range, where stable vortex solitons exist with the local type of nonlinearity derived from the first principles. The latter is true since the nonlinearity in Eq. (1) is calculated from the Schrödinger equation for a Raman medium driven far from the resonance [9,12].

In order to analyze the linear stability we add small perturbations ϵ_n to the vortex solitons and substitute the following ansatz:

$$E_n=[f_n(r)+\epsilon_n(r,\theta,z)]\exp[i(\kappa_1+\kappa_2 n)z+il_n\theta] \tag{9}$$

into Eq. (1). After linearization we find

$$i\partial_z\epsilon_n-\frac{1}{2}\left[\partial_{rr}^2+\frac{1}{r}\partial_r+\frac{1}{r^2}(\partial_{\theta\theta}^2+i2l_n\partial_\theta-l_n^2)\right]\epsilon_n$$
$$=(\kappa_1+p_n)\epsilon_n+q(\epsilon_{n-1}+\epsilon_{n+1})+\sum_m\{A_{nm}\epsilon_m+B_{nm}\epsilon_m^*\}, \tag{10}$$

where

$$A_{nm}=f_{n-1}M_m+f_{n+1}P_m, \tag{11}$$

$$B_{nm}=f_{n-1}P_m+f_{n+1}M_m, \tag{12}$$

$$M_m\equiv\frac{dq^*}{df_m}=\frac{(2\mu^2+s^2)f_{m-1}-s^2f_{m+1}}{4(\mu^2+s^2)^{3/2}}, \tag{13}$$

$$P_m\equiv\frac{dq}{df_m}=\frac{(2\mu^2+s^2)f_{m+1}-s^2f_{m-1}}{4(\mu^2+s^2)^{3/2}}, \tag{14}$$

$n,m=-M+1,\ldots,0,\ldots,N$, and $s=S(f_n)$.

Expanding perturbations into azimutal harmonics [4]

$$\epsilon_n(r,\theta,z)=\sum_{J\geq 0}\{h_{n,J}^+(r,z)\exp(iJ\theta)+[h_{n,J}^-(r,z)]^*\exp(-iJ\theta)\}, \tag{15}$$

we assume $h_{n,J}^{\pm}(r,z)=g_{n,J}^{\pm}(r)\exp(\lambda_J z)$ and derive the eigenvalue problem

$$i\lambda_J\begin{bmatrix}\mathbf{g}_J^+\\ \mathbf{g}_J^-\end{bmatrix}=\begin{bmatrix}L^+ & B\\ -B & -L^-\end{bmatrix}\begin{bmatrix}\mathbf{g}_J^+\\ \mathbf{g}_J^-\end{bmatrix}, \tag{16}$$

where $\mathbf{g}_J^{\pm}=\{g_{1-M,J}^{\pm},\ g_{2-M,J}^{\pm},\ \ldots,\ g_{0,J}^{\pm},\ \ldots,\ g_{N,J}^{\pm}\}^T$. $L^{\pm}$ and B are the $(N+M)\times(N+M)$ matrix operators. Elements of B

are B_{nm} and they are defined in Eq. (12), and the elements of $L^{\pm}$ are

$$L^{\pm}_{nm} = \delta_{n,m}\left[\frac{1}{2r}\frac{d}{dr}\left(r\frac{d}{dr}\right) - \frac{(J \pm l_n)^2}{2r^2} + \kappa_1 + \kappa_2 n + \beta_n\right] + q(\delta_{n+1,m} + \delta_{n-1,m}) + A_{nm}, \tag{17}$$

where $\delta_{n,m}$ is the Kronecker symbol. For a solution f_n to be linearly unstable there must exist λ_J with $\mathrm{Re}(\lambda_J) > 0$. Boundary conditions for eigenstates $\mathbf{g}_J^{\pm}$ are defined in a similar way to the boundary conditions for f_n [see Eqs. (6) and (7)], but with l_n being replaced by $l_n \pm J$. We solve the eigenvalue problem in Eq. (16) numerically, replacing differential operators by the second-order finite differences. Note that accurate stability analysis of the multicomponent solutions is rather complicated. Therefore we will reveal basic mechanisms of instabilities of coupled vortex solitons by focusing on two- and three-component configurations. Then we will demonstrate by numerical modeling of Eqs. (1), that the instability and stabilization mechanisms found in the simplest cases can be seen in the multicomponent dynamics.

V. TWO-COMPONENT VORTEX SOLITONS

We start with the simplest configuration of two sidebands, that is $n=0,1$ ($N=M=1$) in Eqs. (1). This applies, e.g., to the opposite circularly polarized driving fields E_0 and E_1, when the cascaded generation of Stokes and anti-Stokes harmonics is forbidden due to angular momentum selection rules [15]. The propagation equations in this case are

$$\left(i\partial_z - \frac{1}{2}\Delta - \beta_0\right)E_0 = \frac{|E_1|^2 E_0}{2\sqrt{\mu^2 + |E_0|^2|E_1|^2}}, \tag{18}$$

$$\left(i\partial_z - \frac{1}{2}\Delta - \beta_1\right)E_1 = \frac{|E_0|^2 E_1}{2\sqrt{\mu^2 + |E_0|^2|E_1|^2}}. \tag{19}$$

Equations (18) and (19) explicitly express a known fact that the fields interacting via the Raman nonlinearity do not have nonlinear self-action. This property does not depend on the number of interacting components.

Bright (vortex free) spatial solitons in the two-component Raman model have been studied in Refs. [15,16] and the associated self-focusing effects have been observed in Refs. [13,14]. Also, there are closely related recent results on spatial solitons in Raman active liquids [21,22]. The papers in Ref. [23] have analyzed the two-component temporal Raman solitons existing in the presence of group velocity dispersion, i.e., when the transverse Laplacian is replaced with the second-order time derivative. The above two-component model is also similar to that for the so-called holographic solitons [24].

The existence conditions for soliton solutions in Eqs. (8) are reduced to the joint inequalities $\kappa_1 < 0$ and $\kappa_2 < -\kappa_1 - \beta_1$, which define a semi-infinite region in (κ_1, κ_2) bounded by the two rays, see Fig. 3(a). Another boundary is derived from the $q = 1/2$ condition and is given by

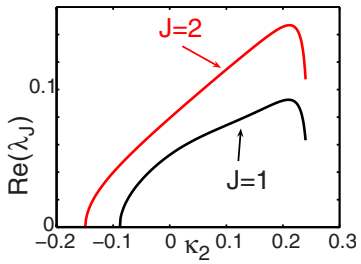

FIG. 4. (Color online) Real part of eigenvalues corresponding to unstable perturbations versus κ_2 for $\kappa_1 = -0.25$.

$$\kappa_2 > \kappa_2^{(s)} = \frac{1}{4\kappa_1} - \kappa_1 - \beta_1. \tag{20}$$

Our linear stability analysis demonstrates that the soliton with $l_0=0$ and $l_1=1$ is unstable only inside the sufficiently narrow range of $\kappa_{1,2}$ corresponding to the relatively small values of q, see Fig. 3. As soon as q increases and the saturation effects become important the solution becomes stable. Note that the saturation of the self-focusing nonlinearity does not stabilize the vortices in the models with the nonlinear self-action effects [4]. It suggests that the absence of the self-action plays an important role in stabilization of the vortex solitons. In its instability range, the vortex soliton is unstable with two eigenvalues $\lambda_{J=1}$ and $\lambda_{J=2}$ having positive real parts, see Fig. 4. Fixing κ_1 we numerically find the critical values of κ_2, at which the two instabilities disappear, see circles and squares in Fig. 3(a). Selective numerical runs for the cases $l_0=0$, $|l_1| \geq 2$ and $l_0=1$, $|l_1| \geq 1$ suggest that they are unstable with respect to azimuthal instabilities through large parts of their existence domains.

To reveal the impact of instabilities on the soliton dynamics, we initialize Eq. (1) with numerically found soliton solutions slightly perturbed along unstable eigenvectors and perform dynamical simulations. Results are presented in Figs. 5 and 6 for the $J=1$ and $J=2$ unstable eigenvectors, respectively. Both perturbations break the soliton symmetry and eventually lead to the formation of a single or a pair of bright spatial solitons [15,16].

VI. THREE-COMPONENT VORTEX SOLITONS

The addition of the third component makes the interaction between the Raman sidebands phase-sensitive, and the choice of the vortex charges l_n in any two fields defines the charge of the remaining field via the phase-matching conditions [11]. Equation (1) for the three component case with $n = 1-M,\ 2-M,\ 3-M$ is

$$\left(i\partial_z - \frac{1}{2}\Delta - \beta_{1-M}\right)E_{1-M} = \frac{C}{2}[|E_{2-M}|^2 E_{1-M} + E_{2-M}^2 E_{3-M}^*], \tag{21}$$

$$\left(i\partial_z - \frac{1}{2}\Delta - \beta_{2-M}\right)E_{2-M} = \frac{C}{2}[(|E_{1-M}|^2 + |E_{3-M}|^2)E_{2-M} + 2E_{3-M}E_{1-M}E_{2-M}^*], \tag{22}$$

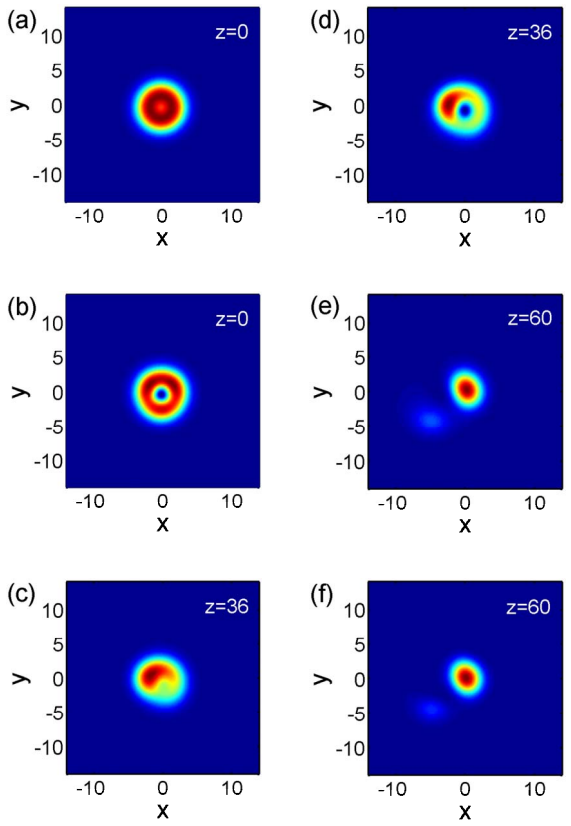

FIG. 5. (Color online) Dynamics of the unstable soliton ($\kappa_1=-0.25$, $\kappa_2=0$) with small perturbation along the $J=1$ unstable eigenvector. Cross sections of field intensities $|E_n|^2$ are plotted for the 0th (left column) and 1st (right column) harmonics at different propagation distances z. The initial soliton has a "donut" shape, which is consistent with the vortex charge $l_1=1$ in the first harmonic. As the instability evolves, it deforms the excitation toward usual bright spatial soliton bearing no vortex charge. Note, that the overall orbital angular momentum is conserved and carried by rapidly diffracting radiative waves.

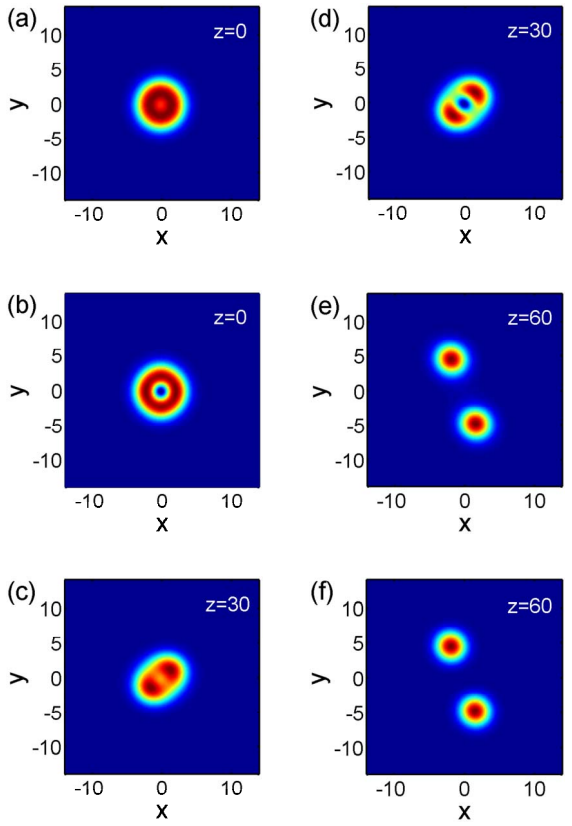

FIG. 6. (Color online) The same as Fig. 5 but with perturbation along $J=2$ unstable eigenvector. As the instability evolves, the soliton is transformed into a pair of spatial solitons, which are then pulled apart and moving in opposite directions.

$$\left(i\partial_z-\frac{1}{2}\Delta-\beta_{3-M}\right)E_{3-M}=\frac{C}{2}[|E_{2-M}|^2E_{3-M}+E_{2-M}^2E_{1-M}^*], \tag{23}$$

here $C^2=1/\{\mu^2+|E_{1-M}E_{2-M}^*+E_{2-M}E_{3-M}^*|^2\}$. Fixing $l_1-l_0=1$, we consider two cases ($M=3$ and $M=2$): asymmetric ($l_{-2}=-2$, $l_{-1}=-1$, $l_0=0$) and symmetric ($l_{-1}=-1$, $l_0=0$, $l_1=1$). The former corresponds to the often encountered case with negligible anti-Stokes sidebands, and the latter implies that the first Stokes and first anti-Stokes lines are excited.

The existence boundary for the asymmetric case given by the condition $q=1/2$ is now $\kappa_2<\kappa_2^{(s)}$, where

$$\kappa_2^{(s)}=-\frac{1}{4}\left[\frac{1}{\kappa_1}-3\kappa_1-2\beta_{-1}-\beta_{-2}-\sqrt{\left(\frac{1}{2\kappa_1}+\beta_{-2}-2\beta_{-1}-\kappa_1\right)^2+2-\frac{1}{4\kappa_1^2}}\right]. \tag{24}$$

In the symmetric case, the $q=1/2$ condition implies $\kappa_2^{(-)}<\kappa_2<\kappa_2^{(+)}$, where

$$\kappa_2^{(\pm)}=\frac{1}{2}\left\{\beta_-\pm\sqrt{\beta_-^2-\frac{\beta_+(1-4\kappa_1^2)}{\kappa_1}-2+4\kappa_1^2}\right\} \tag{25}$$

with $\beta_\pm=(\beta_{-1}\pm\beta_1)$. Together with the conditions in Eqs. (8), the above constraints define the regions of the soliton existence, see Fig. 7.

Stability analysis demonstrates that, similar to the two-component case with $l_0=0$ and $l_1=1$, the three-component solitons with $l_{-2}=-2$, $l_{-1}=-1$, $l_0=0$ are stable inside a sufficiently wide domain in the (κ_1,κ_2) plane and, in particular, in the proximity of the existence boundary given by $q=1/2$, i.e., in the high saturation regime. Close to the lower boundary of the existence domain given by $\kappa_2=(\kappa_1+\beta_{-2})/2$ there are three types of instabilities with $J=1,2,3$, see Fig. 7(a). We note that the solution with the sidebands generated on the anti-Stokes side, i.e., the solution with $l_0=0$, $l_1=1$, $l_2=2$, has the same stability properties as the solution discussed above. The symmetric case with $n=-1,0,+1$ is found to be unstable with respect to the $J=1$ and $J=2$ instabilities, with the former one persisting in the entire existence domain, see Fig. 7(b).

VII. MULTICOMPONENT VORTEX SOLITONS AND SPATIOTEMPORAL HELICAL BEAMS

The above results show that if the vortex soliton contains a vortex free component, for example, at $n=0$, and vortex

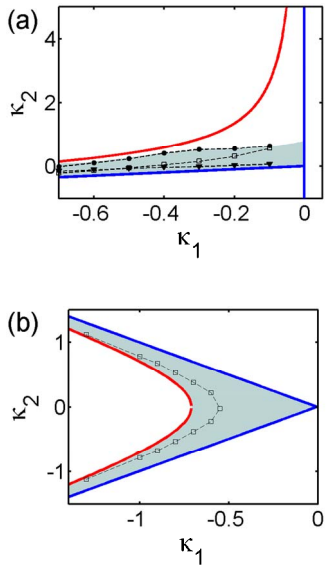

FIG. 7. (Color online) Region of existence of coupled vortex solitons for the case of three fields: (a) asymmetric configuration ($l_{-2}=-2$, $l_{-1}=-1$, $l_0=0$), $\beta_{-1}=0.005$, $\beta_{-2}=0.02$; (b) symmetric configuration ($l_{-1}=-1$, $l_0=0$, $l_1=1$), $\beta_1=\beta_{-1}=0.005$. Open squares, filled circles, and filled triangles correspond to numerically found instability thresholds for $J=1$, $J=2$, and $J=3$ unstable perturbations, respectively. Shaded areas indicate regions of unstable solutions.

carrying sidebands either only on the Stokes or only on the anti-Stokes sides, it can be stable within a broad range of parameters $\kappa_{1,2}$ ensuring that the saturation effects are sufficiently strong. Since in the frequency comb generation experiments with the off-resonant Raman gases the total number of excited harmonics can go to a few dozen [9,10], an important question to be addressed is whether the above stated principles of the vortex soliton stabilization can be extended onto multi-component cases. To address this problem we use numerical integration of Eq. (1) with 11 coupled sidebands, initialized with the three-component vortex solitons described in the previous section. We consider two cases: (i) asymmetric case where excitation of the anti-Stokes lines is suppressed and (ii) symmetric case with excitation of Stokes and anti-Stokes lines being equally probable. In both cases we number the harmonics in a way that $n=0$ corresponds to the vortex-free component. Thus we take $M=11$, $N=0$ and $M=6$, $N=5$ in Eq. (1) for the asymmetric and symmetric cases, respectively.

We monitor the evolution of the fields by plotting the total field intensity $I_{\mathrm{tot}}=|E_{\mathrm{tot}}|^2$ with E_{tot} defined in Eq. (2). It has been demonstrated in Ref. [11] that simultaneous frequency and vortex combs lead to the helical structure of the total field intensity I_{tot}, both in (x,y,t) and (x,y,z) subspaces. For the case of initial conditions where all the fields apart from the three pumps $k-1$, k, and $k+1$ are initially zero, the I_{tot} can be crudely approximated with [see the Appendix for details]:

$$I_{\mathrm{tot}}(x,y,z,t) \approx |f_k^{(0)} + f_{k-1}^{(0)} e^{-i\phi} + f_{k+1}^{(0)} e^{i\phi}|^2, \tag{26}$$

where $\phi=t+\Delta l\theta-Kz$, $\Delta l=l_{k+1}-l_k$ is the vortex charge step between the neighboring sidebands, and $K=\omega_{\mathrm{mod}}L/c-\kappa_2$. For any fixed t and z the total intensity distribution in the transverse plane is modulated in θ with the period defined by Δl, and it rotates in both t and z, forming a spatiotemporal helix.

$\Delta l=1$ corresponds to the single-strand helical structure of I_{tot}, see Figs. 8(a) and 8(b). Figure 8(a) shows the long distance evolution of the helix in the case of the asymmetric excitation, with all the sidebands generated on the Stokes side, see the corresponding spectrum in Fig. 8(c). The resulting helix in this case keeps its structure fixed over considerable propagation lengths. A similar numerical experiment for the symmetric excitation results in the helical soliton, which breaks up into filaments after the same propagation distance, cf. Figs. 8(a) and 8(b). We found that this break up is caused by the developing $j=3$ instability, see Fig. 9. Note, however, that the total length in the simulations shown in Fig. 8 corresponds to a physical distance of order 20 cm, which im-

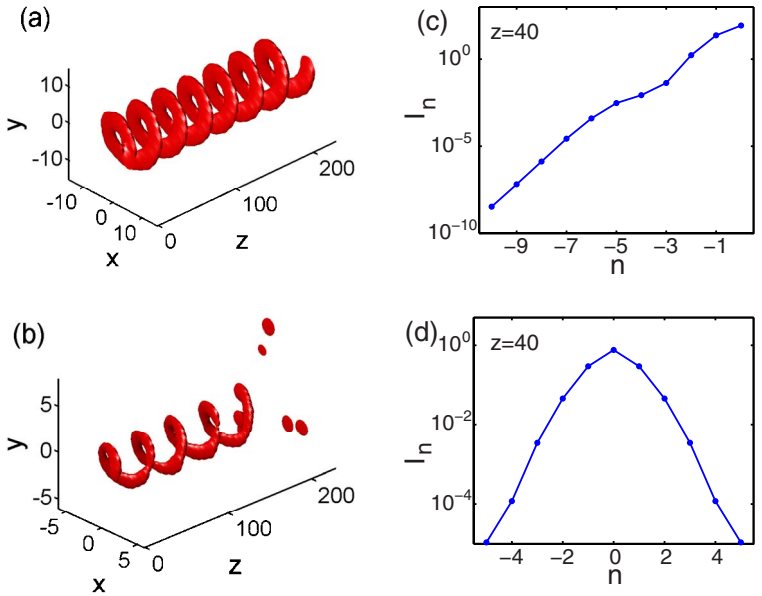

FIG. 8. (Color online) Dynamics of 11 coupled fields initially excited with three-component solitons. (a) $I_{\mathrm{tot}}(x,y,z,t=0)$ isointensity (x,y,z) plot at 80% at maximum for asymmetric configuration. Fields $n=-2,-1,0$ are initialized with the soliton, $\kappa_1=-0.25$, $\kappa_2=0.7$ [stable for three-component configuration, cf. Fig. 7(a)]. (b) The same as (a) but for symmetric configuration, fields $n=-1,0,1$ are excited with the soliton, $\kappa_1=-0.25$, $\kappa_2=0$ [unstable for three-component configuration, cf. Fig. 7(b)]. Isointensity plot is at 60% at maximum; (c) and (d) intensity distribution over harmonics after propagation distance $z=40$ for the cases in (a) and (b), respectively.

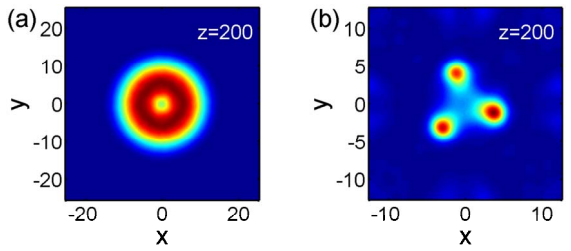

FIG. 9. (Color online) Intensity distribution in the transverse plane of the 0th harmonic after propagation distance $z=200$ for the asymmetric (a) and symmetric (b) configurations in Fig. 8. Impact of the $J=3$ instability in the case of symmetric configuration is clearly observed.

plies that one can speak about a quasistable propagation of the helix even in the case of the symmetric excitation of the Stokes and anti-Stokes sidebands. The z period of the helix $2\pi/K$ is not a parameter of our numerical model, and it is only important when we are calculating E_{tot}. Physically realistic values of the adimensional period are of the order of 1 (for a typical modulation frequency ω_{mod} of the order of 100 GHz [9]), which makes the helical structure contain several hundred periods over the distance of 180 adimensional units required to see the instability. Therefore, to make the structure of the helices and the break-up process more obvious to the reader, we have fixed $K\approx 0.1$, when we have been producing the images of the helices in Figs. 8 and 10.

Providing the asymmetric excitation conditions and changing Δl to 2 and 3, we have also observed the formation of the stable double-and triple-strand helices, see Fig. 10. Note that the formation of similar multiple-strand helices has been reported in Ref. [25], as a result of the linear superposition of the higher order Laguerre-Gauss modes. The helical soliton beams reported here are qualitatively different from

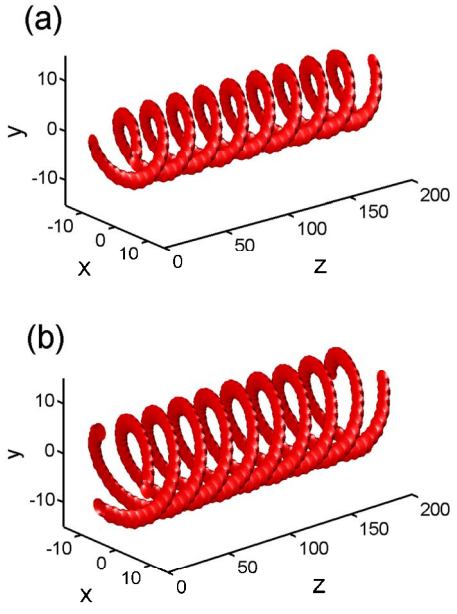

FIG. 10. (Color online) Stable double- (a) and triple-strand (b) helical beams formed by solitons with $\Delta l=2$ and $\Delta l=3$, respectively. All the parameters are the same as in Fig. 8(a).

the so-called spiraling solitons or rotating soliton clusters [26–30], which sustain their rotation due to the interaction between the individual beams accompanied by the conservation of the angular momentum. In our case the helical evolution does not require the presence of more than one intensity lobe, as shown in Fig. 8, and originates from the interaction of multiple frequency harmonics carrying progressively growing vortex charges. Most close known to us analog of the spatiotemporal helices studied above have been reported in the context of the sine Gordon equation and can be observed in a chain of coupled pendulums [31].

VIII. SUMMARY

In this work we have reported existence conditions and have carried out linear stability analysis of the two and three component vortex solitons in an off-resonant Raman medium. We have found that, in the case where the vortex carrying Raman side bands are located either only on the Stokes or only on the anti-Stokes side of the vortex free component, the vortex solitons have a significant stability domain, corresponding to parameter values ensuring sufficient levels of nonlinearity saturation. We have also demonstrated that the same stabilization mechanisms work in the case of many sideband, leading to the excitation of stable helical beams with single-, double-, and triple-strand topologies.

APPENDIX

An approximate expression for the z evolution of the simultaneous frequency and vortex combs, excited with finite number of the sidebands, can be found if one neglects diffraction and dispersion. We replace Eq. (4) with $E_n(x,y,z)\approx f_n(z)e^{il_n\theta}$ and use the fact that under these approximations

$$i\frac{\partial f_n}{\partial z}=q(f_{n+1}-f_{n-1}). \tag{A1}$$

A solution to an initial value problem for Eqs. (A1) can be expressed using the Bessel functions $J_n(z)$. For an initial excitation with N_0 adjacent sidebands: $f_n^{(0)}\neq 0$ for $n=k,k+1,\ldots,k+N_0-1$, the resulting solution is given by

$$f_n(z)=\sum_{j=k}^{k+N_0-1} f_j^{(0)}e^{-i\pi(n-j)/2}J_{n-j}(2q_0z), \tag{A2}$$

where $q_0=q(z=0)$. The simplest case $N_0=2$ has been considered in Refs. [9,11]. Using the orthogonality of the Bessel functions $\Sigma_n J_{n+p}J_{n+q}=\delta_{p,q}$, it is easy to show that $q(z)\equiv q_0$ and thus Eq. (A2) satisfies Eq. (A1) for all z. Substituting the solution (A2) into Eq. (2), we find the approximate expression for the total field

$$E_{\mathrm{tot}} \approx \exp(i\phi_0)\sum_n \{\exp[in\phi] \times \sum_{j=k}^{k+N_0-1} f_j^{(0)} e^{-i\pi(n-j)/2} J_{n-j}(2q_0 z)\}, \quad \text{(A3)}$$

where $\phi_0 = l_0\theta + \omega_0 t/\omega_{\mathrm{mod}} - K_0 z$, $\phi = \Delta l\theta + t - Kz$, $K_0 = \omega_0 L/c - \kappa_1$, $K = \omega_{\mathrm{mod}} L/c - \kappa_2$. Using a known identity, $\Sigma_n J_n(x)\exp(in\alpha) = \exp[ix\sin(\alpha)]$, we derive

$$E_{\mathrm{tot}} \approx \exp[i\phi_0 + i2q_0 z\cos(\phi)] \sum_{j=k}^{k+N_0-1} f_j^{(0)} \exp[ij\phi], \quad \text{(A4)}$$

which is the expression used in Eq. (26).

[1] A. S. Desyatnikov and Y. S. Kivshar, Prog. Opt. **47**, 219 (2005).
[2] A. V. Buryak, P. Di Trapani, D. V. Skryabin, and S. Trillo, Phys. Rep. **370**, 63 (2002).
[3] K. Dholakia, N. B. Simpson, M. J. Padgett, and L. Allen, Phys. Rev. A **54**, R3742 (1996).
[4] D. V. Skryabin and W. J. Firth, Phys. Rev. E **58**, 3916 (1998).
[5] J. P. Torres, J. M. Soto-Crespo, L. Torner, and D. V. Petrov, Opt. Commun. **149**, 77 (1998).
[6] P. Di Trapani, W. Chinaglia, S. Minardi, A. Piskarskas, and G. Valiulis, Phys. Rev. Lett. **84**, 3843 (2000).
[7] D. Mihalache, D. Mazilu, I. Towers, B. A. Malomed, and F. Lederer, Phys. Rev. E **67**, 056608 (2003).
[8] S. Sogomonian, U. T. Schwarz, and M. Maier, J. Opt. Soc. Am. B **18**, 497 (2001).
[9] A. V. Sokolov and S. E. Harris, J. Opt. B: Quantum Semiclassical Opt. **5**, R1 (2003).
[10] A. M. Burzo, A. V. Chugreev, and A. V. Sokolov, Opt. Commun. **264**, 454 (2006).
[11] A. V. Gorbach and D. V. Skryabin, Phys. Rev. Lett. **98**, 243601 (2007).
[12] A. V. Gorbach and D. V. Skryabin, Opt. Lett. **31**, 3309 (2006).
[13] N. A. Proite, B. E. Unks, J. T. Green, and D. D. Yavuz, Phys. Rev. A **77**, 023819 (2008).
[14] D. R. Walker, D. D. Yavuz, M. Y. Shverdin, G. Y. Yin, A. V. Sokolov, and S. E. Harris, Opt. Lett. **27**, 2094 (2002).
[15] D. D. Yavuz, D. R. Walker, and M. Y. Shverdin, Phys. Rev. A **67**, 041803(R) (2003).
[16] D. D. Yavuz, Phys. Rev. A **75**, 041802(R) (2007).
[17] J. M. Soto-Crespo, D. R. Heatley, E. M. Wright, and N. N. Akhmediev, Phys. Rev. A **44**, 636 (1991); J. Atai, Y. Chen, and J. M. Soto-Crespo, *ibid.* **49**, R3170 (1994); V. Tikhonenko, J. Christou, and B. LutherDavies, J. Opt. Soc. Am. B **12**, 2046 (1995); B. A. Malomed and A. A. Nepomnyashchy, Phys. Rev. E **52**, 1238 (1995).
[18] D. Briedis, D. E. Petersen, D. Edmundson, W. Krolikowski, and O. Bang, Opt. Express **13**, 435 (2005).
[19] S. Skupin, M. Saffman, and W. Krolikowski, Phys. Rev. Lett. **98**, 263902 (2007).
[20] D. Mihalache, D. Mazilu, L. C. Crasovan, I. Towers, B. A. Malomed, A. V. Buryak, L. Torner, and F. Lederer, Phys. Rev. E **66**, 016613 (2002).
[21] G. Fanjoux, J. Michaud, M. Delque, H. Maillotte, and T. Sylvestre, Opt. Lett. **31**, 3480 (2006).
[22] G. Fanjoux, J. Michaud, H. Maillotte, and T. Sylvestre, Phys. Rev. Lett. **100**, 013908 (2008).
[23] D. V. Skryabin, F. Biancalana, D. M. Bird, and F. Benabid, Phys. Rev. Lett. **93**, 143907 (2004); D. V. Skryabin and A. V. Yulin, Phys. Rev. E **74**, 046616 (2006).
[24] O. Cohen, T. Carmon, M. Segev, and S. Odoulov, Opt. Lett. **27**, 2031 (2002).
[25] S. Franke-Arnold, J. Leach, M. J. Padgett, V. E. Lembessis, D. Ellinas, A. J. Wright, J. M. Girkin, P. Ohberg, and A. S. Arnold, Opt. Express **15**, 8619 (2007).
[26] A. V. Buryak, Y. S. Kivshar, M. F. Shin, and M. Segev, Phys. Rev. Lett. **82**, 81 (1999).
[27] T. Carmon, R. Uzdin, C. Pigier, Z. H. Musslimani, M. Segev, and A. Nepomnyashchy, Phys. Rev. Lett. **87**, 143901 (2001).
[28] A. S. Desyatnikov and Y. S. Kivshar, Phys. Rev. Lett. **88**, 053901 (2002).
[29] D. V. Skryabin, J. M. McSloy, and W. J. Firth, Phys. Rev. E **66**, 055602(R) (2002).
[30] Y. V. Kartashov, L. C. Crasovan, D. Mihalache, and L. Torner, Phys. Rev. Lett. **89**, 273902 (2002).
[31] M. Remoissenet, *Waves Called Solitons* (Springer, Berlin, 1999), Chap. 6.